

Spin Waves in Striped Phases

E. W. Carlson¹, D. X. Yao², and D. K. Campbell²

(1) Dept. of Physics, Purdue University, West Lafayette, IN 47907

(2) Dept. of Physics and Dept. of Electrical and Computer Engineering, Boston University, Boston, MA 02215

(Dated: March 22, 2022)

In many antiferromagnetic, quasi-two-dimensional materials, doping with holes leads to “stripe” phases, in which the holes congregate along antiphase domain walls in the otherwise antiferromagnetic texture. Using a suitably parametrized two-dimensional Heisenberg model on a square lattice, we study the spin wave spectra of well-ordered spin stripes, comparing bond-centered antiphase domain walls to site-centered antiphase domain walls for a range of spacings between the stripes and for stripes both aligned with the lattice (“vertical”) and oriented along the diagonals of the lattice (“diagonal”). Our results establish that there are qualitative differences between the expected neutron scattering responses for the bond-centered and site-centered cases. In particular, bond-centered stripes of odd spacing generically exhibit more elastic peaks than their site-centered counterparts. For inelastic scattering, we find that bond-centered stripes produce more spin wave bands than site-centered stripes of the same spacing and that bond-centered stripes produce rather isotropic low energy spin wave cones for a large range of parameters, despite local microscopic anisotropy. We find that extra scattering intensity due to the crossing of spin wave modes (which may be linked to the “resonance peak” in the cuprates) is more likely for diagonal stripes, whether site- or bond-centered, whereas spin wave bands generically repel, rather than cross, when stripes are vertical.

I. INTRODUCTION

Many doped strongly correlated materials exhibit evidence for an emergent length scale in the form of “stripes”, i.e., regular antiphase domain walls in an otherwise antiferromagnetic texture. The strongest evidence for striped structures in nickelate perovskites and some related cuprates has come from neutron scattering,^{1,2,3,4,5} which is capable of detecting the spin texture directly through diffraction. Since several theories of high temperature superconductivity make contact with such structures,^{6,7,8,9,10,11,12} it is important to improve our microscopic picture of them. In particular, it is not yet known from experiment whether the antiphase domain walls sit primarily on nickel (copper) sites, or rather sit primarily on oxygen sites.

When undoped, the nickel-oxygen (and copper-oxygen) planes in these materials are antiferromagnetic, with spin moments localized on the Ni (Cu) sites, as evidenced by a peak in elastic neutron scattering at (π, π) .¹³ Upon hole doping, this peak is observed to split into four (or perhaps two^{14,15}) “incommensurate peaks”,¹⁶ indicating an extra modulation on top of the antiferromagnetic wavelength. For the case of collinear spins, this is consistent with the formation of periodic antiphase domain walls in the antiferromagnetic texture (*i.e.* stripes).

On a two-dimensional square lattice, these domains consist of a strip of antiferromagnet with spin up on, say, the “A” sublattice, separated by a domain wall from a strip of antiferromagnet with spin up on the “B” sublattice, and so on, as in Fig. 1. The figures necessarily depict a certain width for each antiphase domain wall, but the widths are not known and are in reality likely less sharp than shown in the figure. In both cases, neighboring antiferromagnetic patches have spin

up on opposite sublattices, which washes out any signal at the antiferromagnetic peak (π, π) . Rather, satellite peaks are observed around (π, π) , at a distance determined by the spacing between domain walls. When the domain walls are site-centered, all couplings are antiferromagnetic, including couplings across the domain walls. Bond-centered domain walls, however, have some ferromagnetic couplings.¹⁷ That is, bond-centered configurations consist of antiferromagnetic patches which are *ferromagnetically* coupled across the domain wall. As shown in Fig. 1, we consider stripes aligned with the lattice direction (called “vertical stripes”) or aligned along the lattice diagonals (called “diagonal stripes”).

In this article we focus on the spin wave spectra and expected magnetic scattering intensities of bond-centered and site-centered stripe phases of various spacings and orientations. Other stripe phases are certainly possible, such as phases which mix site- and bond-centered domain walls, or phases in which the spacing of the antiphase domain walls is not commensurate with the underlying lattice, or “dynamic” stripes¹⁸, which fluctuate in time. We will not consider these cases here, but focus on well-ordered spin stripes which have purely site- or bond-centered domain walls. As we will show below, there are qualitative differences between the spin wave spectra of bond- and site-centered domain walls, indicating that in some cases inelastic neutron scattering may be able to distinguish between the two. In addition, there is a difference in the number of peaks in the elastic spin structure factor for odd stripe spacings, indicating that elastic neutron scattering alone may be able to distinguish as well.

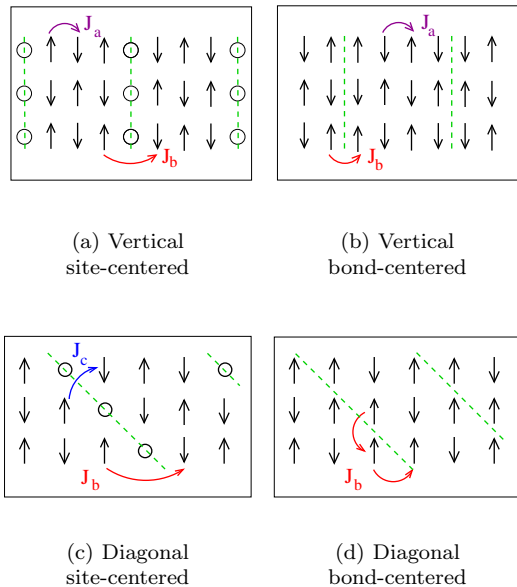


FIG. 1: (Color online) (a) Site-centered vertical stripe pattern with $p = 4$ lattice constants between domain walls. In this configuration, exchange couplings $J_a > 0$ and $J_b > 0$ are all antiferromagnetic. (b) Bond-centered vertical stripe pattern with spacing $p = 4$. The exchange coupling $J_a > 0$ is antiferromagnetic, while $J_b < 0$ is ferromagnetic. (c) Diagonal site-centered domain walls have coupling $J_b > 0$ for next nearest neighbor spins coupled across the domain wall along the vectors $(2, 0)$ and $(0, 2)$, and coupling $J_c > 0$ diagonally to “Manhattan” second neighbors across the domain walls along the vector $(1, 1)$, in units where the square lattice spacing $a = 1$. (d) Diagonal bond-centered domain walls have nearest neighbor ferromagnetic coupling $J_b < 0$ across the domain wall. The size of each figure has been chosen for visual clarity.

II. MODEL

We consider static, ordered arrays of antiphase domain walls in an otherwise antiferromagnetic texture. Although the domain walls collect charge^{19,20,21,22}, we neglect this charge component, as we are interested solely in the response of the spin degrees of freedom. We use a Heisenberg model on a two-dimensional square lattice:

$$H = \frac{1}{2} \sum_{\langle \mathbf{r}, \mathbf{r}' \rangle} J_{\mathbf{r}, \mathbf{r}'} \mathbf{S}_{\mathbf{r}} \mathbf{S}_{\mathbf{r}'}, \quad (1)$$

where $\langle \mathbf{r}, \mathbf{r}' \rangle$ runs over all spin sites, and the exchange coupling is $J_{\mathbf{r}, \mathbf{r}'}$. Within an antiferromagnetic patch, nearest neighbor couplings are antiferromagnetic with $J_{\mathbf{r}, \mathbf{r}'} = J_a > 0$. Couplings across a domain wall depend upon the configuration and are enumerated below. All other couplings are neglected. When comparing to the nickel oxides (copper oxides), our lattice corresponds to the nickel (copper) sites within the nickel-oxygen (copper-oxygen) planes.

A. Vertical Stripes

We consider first the case where stripes run parallel to the Ni-O (Cu-O) bond direction; we call these “vertical” stripes. As illustrated in Fig. 1, when the domain wall is centered on a lattice site, we may describe the system as having no net spin on the domain wall.²³ In this case, spins from the edges of neighboring antiferromagnetic patches are coupled across the domain wall *antiferromagnetically*, $J_{\mathbf{r}, \mathbf{r}'} = J_b > 0$ with $\mathbf{S}_{\mathbf{r}} = 0$ on the domain wall, as illustrated in Fig. 1(a). Within the antiferromagnetic patches, nearest neighbor spins are of course also antiferromagnetically coupled, $J_{\mathbf{r}, \mathbf{r}'} = J_a > 0$. When, however, the domain wall is bond-centered—that is, situated between two sites as in Fig. 1(b)—spins from the edges of neighboring antiferromagnetic patches are *ferromagnetically* coupled, and we have $J_{\mathbf{r}, \mathbf{r}'} = J_b < 0$ across the domain wall. Nearest neighbor exchange couplings within each antiferromagnetic patch remain antiferromagnetic, $J_{\mathbf{r}, \mathbf{r}'} = J_a > 0$. We shall see that this ferromagnetic coupling J_b of spins across the domain wall leads to distinctive features for the spin waves in the bond-centered case.

We define the magnetic Bravais lattice as follows.²⁴ Let p denote the distance between domain walls. We will henceforth work in units where the square lattice spacing $a = 1$. For $p = \text{odd}$, we choose the basis vectors $\mathbf{A}_1 = (p, 0)$ and $\mathbf{A}_2 = (0, 2)$, and for $p = \text{even}$, we use $\mathbf{A}_1 = (p, 1)$ and $\mathbf{A}_2 = (0, 2)$. For site-centered configurations, there are $N = 2p$ sites within each unit cell which include $2(p-1)$ spins and 2 sites with no static spin component. For bond-centered domain walls, there are $N = 2p$ spins in each unit cell. (See Fig. 2.)

We use the notation VS_p and VB_p to refer to vertical stripes of spacing p in a site(S)- or bond(B)-centered configuration, respectively. For example, VS_3 refers to a vertical site-centered configuration with spacing $p = 3$ between domain walls.

B. Diagonal Stripes

For diagonal stripes, the antiphase domain walls are oriented along the $(1, \pm 1)$ direction in a square lattice (recall we have set the lattice spacing $a = 1$). For the same microscopic interaction strengths (deriving $J_{\mathbf{r}, \mathbf{r}'}$ from, *e.g.*, a Hubbard model), spins are more strongly coupled across the domain wall than in the vertical case. For example, with diagonal bond-centered stripes, each spin neighboring the domain wall interacts with *two* nearest neighbor (ferromagnetically coupled) spins across the domain wall, as shown in Fig. 1(d). Contrast this with the vertical stripes of Fig. 1(a) and (b), where each spin neighboring a domain wall interacts with only one spin across the domain wall. Diagonal site-centered stripes are even more strongly coupled, with two different types of interactions across the domain wall, one of which we label J_b because it connects spins along a bond direction

(connecting spins along the vectors $(2, 0)$ and $(0, 2)$ across the domain wall), and the other we label J_c (connecting spins along the vector $(1, 1)$ across the domain wall), as shown in Fig. 1(c).

For diagonal stripes, the magnetic Bravais lattice differs from the vertical case. For $p = \text{odd}$ spacing between domain walls, we choose the basis vectors $\mathbf{A}_1 = (p, 0)$ and $\mathbf{A}_2 = (-1, 1)$, and for $p = \text{even}$, we use $\mathbf{A}_1 = (2p, 0)$ and $\mathbf{A}_2 = (-1, 1)$. For site-centered configurations, when p is even there are $N = 2p$ sites within each unit cell which includes $2(p - 1)$ spins and 2 sites with no static spin component, and when p is odd, there are $N = p$ sites within each unit cell, which includes $p - 1$ spins, and one empty site. For bond-centered domain walls, there are $N = 2p$ spins in each unit cell when p is even, and there are $N = p$ spins in the unit cell when p is odd. (See Fig. 7.)

We use the notation DSp and DBp to refer to diagonal stripes of spacing p in a site (S)- or bond (B)-centered configuration, respectively.

III. SPIN WAVE THEORY

The elementary excitations of ordered spin textures may be studied using the well-known technique of Holstein-Primakoff bosons. The same dispersion is obtained by quantizing the classical spin waves, and the methods are equivalent as $S \rightarrow \infty$. We use each description when convenient. As it is physically more transparent, we review here the latter method²⁵, discussing the former in Appendix A.

In the classical spin wave approach, each spin is treated as precessing in the effective field produced by its coupled neighbors, via the torque equations of a spin in a magnetic field.²⁵ The rate of change of the spin at position \mathbf{r} is described by

$$\hbar \frac{d\mathbf{S}_{\mathbf{r}}}{dt} = \mu_{\mathbf{r}} \times \mathbf{H}_{\mathbf{r}}^{\text{eff}}, \quad (2)$$

where $\mu_{\mathbf{r}}$ and $\mathbf{H}_{\mathbf{r}}^{\text{eff}}$ are respectively the corresponding magnetic moment and effective magnetic field at position \mathbf{r} , defined by

$$\begin{aligned} \mu_{\mathbf{r}} &= -g\mu_B \mathbf{S}_{\mathbf{r}} \\ \mathbf{H}_{\mathbf{r}}^{\text{eff}} &= \frac{1}{g\mu_B} \sum_{\mathbf{r}'} J_{\mathbf{r},\mathbf{r}'} \mathbf{S}_{\mathbf{r}'}, \end{aligned} \quad (3)$$

Within our model, Eqn. (1), the torque equations become

$$\begin{aligned} \frac{dS_{\mathbf{r}}^x}{dt} &= -\frac{1}{\hbar} (S_{\mathbf{r}}^y \sum_{\mathbf{r}'} J_{\mathbf{r},\mathbf{r}'} S_{\mathbf{r}'}^z - S_{\mathbf{r}}^z \sum_{\mathbf{r}'} J_{\mathbf{r},\mathbf{r}'} S_{\mathbf{r}'}^y) \\ \frac{dS_{\mathbf{r}}^y}{dt} &= -\frac{1}{\hbar} (S_{\mathbf{r}}^z \sum_{\mathbf{r}'} J_{\mathbf{r},\mathbf{r}'} S_{\mathbf{r}'}^x - S_{\mathbf{r}}^x \sum_{\mathbf{r}'} J_{\mathbf{r},\mathbf{r}'} S_{\mathbf{r}'}^z) \\ \frac{dS_{\mathbf{r}}^z}{dt} &\approx 0, \end{aligned} \quad (4)$$

where we have assumed large S and small oscillations, so that changes in S^z can be neglected. We seek solutions of the form

$$\begin{aligned} S_{\mathbf{r}}^x &= S_i^x \exp[i(\mathbf{k} \cdot \mathbf{r} - \omega t)] \\ S_{\mathbf{r}}^y &= S_i^y \exp[i(\mathbf{k} \cdot \mathbf{r} - \omega t)] \end{aligned} \quad (5)$$

where i labels spins within the unit cell, i.e. $i = 1, 2, \dots, N$; N is the total number of spins in the unit cell; $\mathbf{k} = (k_x, k_y)$, and $\mathbf{r} = (r_x, r_y)$. Setting the determinant of the coefficients of S_i^x and S_i^y to zero yields the dispersion relations for the spin wave.

We calculate the zero-temperature dynamic structure factor using Holstein-Primakoff bosons.

$$S(\mathbf{k}, \omega) = \sum_f \sum_{i=x,y,z} |\langle f | S^i(\mathbf{k}) | 0 \rangle|^2 \delta(\omega - \omega_f) \quad (6)$$

Here $|0\rangle$ is the magnon vacuum state and $|f\rangle$ denotes the final state of the spin system with excitation energy ω_f . Since S^z does not change the number of magnons, it leads to the elastic part of the structure factor. Single magnon excitations contribute to the inelastic response through $\mathbf{S}^x(\mathbf{k})$ and $\mathbf{S}^y(\mathbf{k})$.

IV. RESULTS FOR VERTICAL STRIPES

We begin with our results for ordered, vertical stripe phases. We discuss magnon excitation energies as functions of momentum, the dynamic spin structure factors, the elastic response, the velocities of the acoustic bands, and analytic results for dispersion relations for small unit cell sizes. Fig. 2 shows schematic representations of vertical stripes that are site- and bond-centered, with both even and odd spacing. In this figure (in contrast to Fig. (1)) we have used the length of the arrow to represent the net spin on a site. The net spin is expected to be smaller near domain walls (as it is always zero on a domain wall). Our zero frequency results incorporate this general form factor. For the finite ω results, we use a form factor with the same net spin on each occupied site.

A. Elastic peak at $(0, \pi)$

Elastic neutron scattering can in principle detect one important qualitative difference between bond- and site-centered stripes. For odd stripe spacings, both bond- and site-centered stripes have magnetic reciprocal lattice vectors at $(0, \pi)$. However, site-centered stripes are forbidden from producing weight at $(0, \pi)$, whereas bond-centered stripes generically show weight at this point. This is related to the discrete Fourier transform of the spin structure. Taking advantage of the antiferromagnetic long range order in one direction and the finite

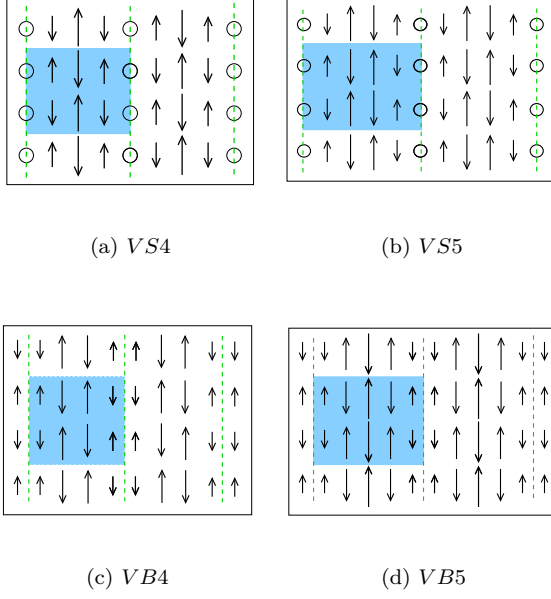


FIG. 2: (Color online) Vertical site- and bond-centered configurations, showing even and odd spacing. “S” refers to site-centered configurations, and “B” refers to bond-centered configurations. The number label is the spacing p between domain walls. Dotted vertical lines mark antiphase domain walls. The solid boxes denote unit cells. The height of the arrows represents the net spin on a site, which is expected to peak between domain walls.

spacing between stripes in the other, we can describe the spin structure in real space by a function

$$S^z(n, m) = \cos(\pi m) \sum_{j=0}^{j'} A_j e^{i \frac{2\pi j}{p} n} \quad (7)$$

$$= f(n)g(m), \quad (8)$$

where m is the discrete y coordinate parallel to the stripes, n is the discrete x coordinate perpendicular to them, and where $j' = p-1$ for p odd, with $j' = 2p-1$ for p even. The functions $f(n)$ and $g(m)$ are shown schematically in Fig. 3. The elastic scattering cross section is proportional to the Fourier transform of $S^z(n, m)$:²⁶

$$\left(\frac{d\sigma}{d\Omega} \right)_{el} \propto \sum_{m,n} e^{i(k_m m + k_n n)} \langle S^z(m, n) \rangle \langle S^z(0, 0) \rangle \quad (9)$$

$$= \sum_m e^{ik_m m} \cos(\pi m) \sum_{j=0}^{j'} A_j \sum_n e^{ik_n n} e^{i \frac{2\pi j}{p} n}$$

$$= N_m (\delta_{k_m, \pi} + \delta_{k_m, -\pi}) \sum_{j=0}^{j'} A_j \sum_n N_n \delta_{k_n, -\frac{2\pi j}{p}}.$$

We emphasize that this expression allows for *any form factor* and is not restricted to configurations where each

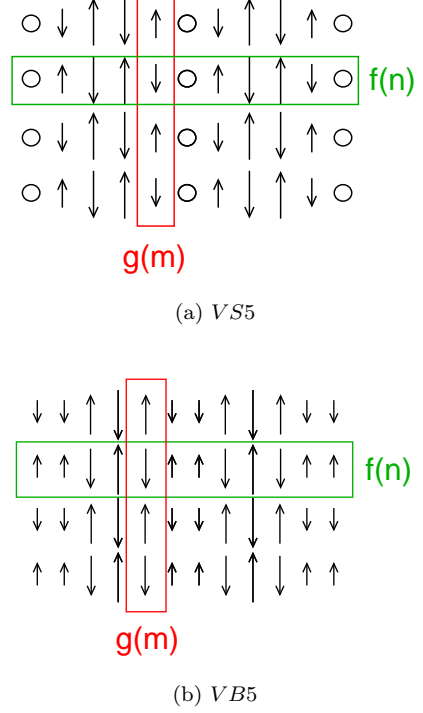


FIG. 3: (Color online) Schematic representation of vertical stripes with $p = \text{odd}$ widths, indicating the pattern of the functions $g(m)$ and $f(n)$. Note that for the bond-centered case with odd stripe spacings, the function $f(n)$ can have a net magnetization, producing elastic weight at the peak $(0, \pi)$.

occupied site has a full quantum of spin. In the case where each occupied site has the same net spin, the ratio of intensity at the main peaks $(\pi \pm \pi/p, \pi)$ to that at $(0, \pi)$ is 2 in the VB3 case, and 2.6 in the VB5 case. Site-centered stripes always have $A_0 = 0$, while A_0 is generically nonzero for bond-centered stripes (although it can be fine-tuned to zero). A finite $j = 0$ term produces elastic weight at $(0, \pi)$. This can be understood heuristically from considering the function $f(n)$, shown schematically for the VB5 case in Fig. 3. Odd-spacing bond-centered stripes generically have a net magnetization in the function $f(n)$, while symmetry forbids this for site-centered stripes.

B. Analytic Results for small p

For small p , which corresponds to small unit cell sizes, we can obtain analytic results for the dispersion relation of the acoustic mode. For the case VS3, we find

$$\left(\frac{\omega_{VS3}}{J_a S} \right)^2 = 4(\lambda + 1) + C - 4(\lambda + 1)D \quad (10)$$

where

$$\lambda = \left| \frac{J_b}{J_a} \right| \quad (11)$$

$$C = 2\lambda f(3k_x) + 8f(k_y) - 4f^2(k_y)$$

$$D = |1 - f(k_y)| \sqrt{1 - \frac{2\lambda f(3k_x)}{(\lambda + 1)^2}}$$

and the function f is defined as

$$f(x) = 1 - \cos(x) . \quad (12)$$

The acoustic spin wave velocity parallel to the stripe direction ($\mathbf{k} \parallel \hat{y}$) may be obtained by setting $k_x = 0$ above, and taking $k_y \ll 1$. In this case, $f(k_x) = 0$, $f(k_y) \rightarrow \frac{1}{2}k_y^2$, and $\omega_{VB2} \rightarrow v_{\parallel}|k_y|$, where

$$v_{\parallel} = \frac{1}{2}\sqrt{\lambda + 3} v_{AF}, \quad (13)$$

and $v_{AF} = 2\sqrt{2}J_a S$ is the velocity of the pure antiferromagnet with coupling J_a and no antiphase domain walls. The spin wave velocity perpendicular to the stripe direction may be similarly obtained:

$$v_{\perp} = \frac{3\sqrt{2}}{4} \sqrt{\frac{\lambda(\lambda + 3)}{\lambda + 1}} v_{AF}. \quad (14)$$

For $\lambda \gg 1$, these approach $v_{\perp} \rightarrow (3/\sqrt{2})\sqrt{\lambda} v_{AF}$ and $v_{\parallel} \rightarrow (1/2)\sqrt{\lambda} v_{AF}$.

For the case VB2, the problem reduces to diagonalizing a 4×4 matrix, with the result

$$\left(\frac{\omega_{VB2}}{J_a S} \right)^2 = 2(\lambda^2 + 3\lambda + 2) + A - 2\sqrt{(\lambda^2 + 3\lambda + 2)^2 + B} \quad (15)$$

where

$$A = 2f(2k_y) \quad (16)$$

$$B = -\frac{1}{2}\lambda^2 f(4k_x) - 4f(k_y) - 4(\lambda^2 + 3\lambda)f(2k_x) - 4f(k_y)(1 - f(k_y) + (\lambda^2 + 3\lambda)(1 - f(2k_x))).$$

The spin wave velocities in the case VB2 are

$$v_{\parallel} = \frac{\sqrt{3}}{2} v_{AF}, \quad (17)$$

independent of λ , and

$$v_{\perp} = \sqrt{\frac{3\lambda}{2(\lambda + 1)}} v_{AF}. \quad (18)$$

For $\lambda \gg 1$, we note that v_{\perp} saturates at

$$v_{\perp} \rightarrow \sqrt{\frac{3}{2}} v_{AF}. \quad (19)$$

That v_{\perp} saturates with large λ is in contrast to the behavior of site-centered cases and can lead to rather isotropic spin wave cones for the bond-centered case,^{3,4} despite local microscopic anisotropy. As discussed in the next section, for bond-centered stripes with any spacing p , v_{\parallel} is independent of λ and v_{\perp} saturates with large λ .

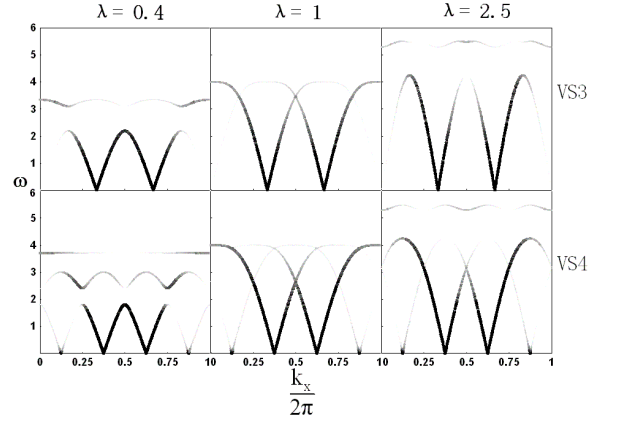


FIG. 4: Spin wave spectra and intensities for vertical, site-centered stripes. All spectra are reported at $k_y = \pi$ as a function of the transverse momentum k_x . The frequency ω is in units of $J_a S$. Apparent crossings only occur at $\lambda = 1$ and $\lambda = 2.5$.

C. Numerical Results

For most values of the stripe spacing p , the spin wave matrices are sufficiently large that one must use numerical diagonalizations to obtain the dispersion relations of the various modes. From the corresponding eigenfunctions we can then also calculate the spectral intensity (proportional to the dynamic structure factor) that these magnon states would contribute to the inelastic neutron scattering. Figs. 4 and 5 show the calculated dispersion and scattering intensities for site- and bond-centered stripes of various spacings. Our results for site-centered stripes are consistent with those of Ref.²⁴. For the site-centered case, bands never cross for $\lambda < 1$. At the critical couplings $\lambda = 1$ and $\lambda = 2.5$, site-centered bands appear to cross. Away from these couplings, vertical site-centered bands generally repel rather than cross. For $\lambda = 1$, the dispersion is very similar to that of a pure antiferromagnet, albeit with different magnetic reciprocal lattice vectors. For any coupling λ , as $p \rightarrow \infty$, the result for a pure 2D antiferromagnet is recovered. For p increasing but finite, the number of bands as well as the number of reciprocal lattice vectors increases. However as $p \rightarrow \infty$, all spectral weight is transferred to the response of a pure antiferromagnet.

Fig. 5 shows representative results for vertical bond-centered antiphase domain walls with spacings $p = 2, 3$, and 4. In this case, the critical point where bands appear to touch is at $\lambda_c \approx 0.56$ and is at most only weakly dependent on p . Away from the critical coupling, bands never appear to cross, but rather level repulsion is observed. There are other notable differences between the site- and bond-centered cases. For one thing, for the same spacing p , bond-centered configurations yield one more band: site-centered configurations have $p - 1$ bands, whereas there are p bands for bond-centered configurations.

A qualitative difference between the two cases is the

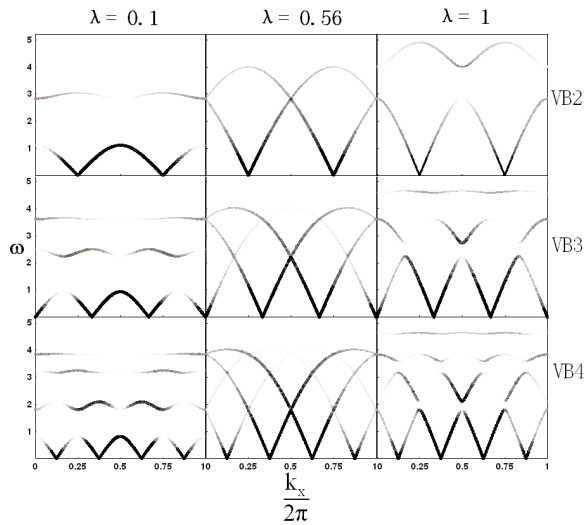


FIG. 5: Spin wave spectra and intensities for vertical, bond-centered stripes. All spectra are reported at $k_y = \pi$ as a function of the transverse momentum k_x . The frequency ω is in units of $J_a S$.

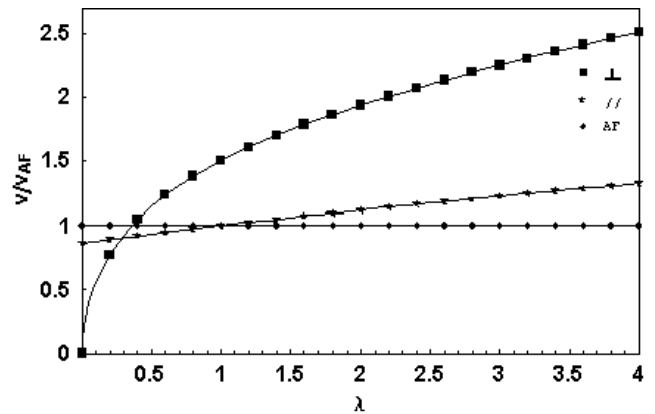
scaling of the band energies with coupling λ . For site-centered configurations, all bands increase their energy monotonically with the coupling ratio λ . This is in contrast with the bond-centered case, where for large J_b , only the top band is affected by the ferromagnetic coupling (that is, it increases linearly with λ), but all other bands saturate as λ is increased. The behavior of the top band can be understood by considering the spins that are ferromagnetically coupled across the domain wall. In the top band, these spins precess π out of phase with each other, and the dispersion is dominated by the behavior of the effective ferromagnetic dimers, yielding $\omega \rightarrow 2|J_b|S/\hbar$ as $|J_b| \rightarrow \infty$, as shown in Appendix B.

An important consequence of the saturation of the lower bands as λ gets large in the bond-centered cases is that the low-energy spin wave velocities alone, v_\perp and v_\parallel , cannot readily be used to extract the relation between the bare exchange couplings J_a and J_b . We explore this point in more detail in the next section.

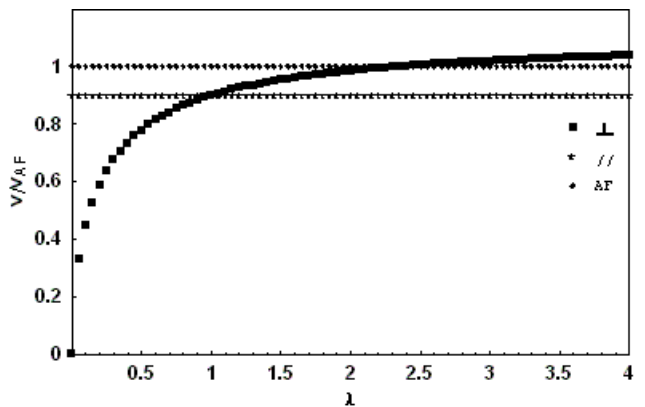
In Fig. 6 we present the spin wave velocities perpendicular (v_\perp) and parallel (v_\parallel) to the stripe orientation for the acoustic (lowest) bands as functions of the coupling constant ratio λ . These are compared to the reference velocity, v_{AF} of the pure antiferromagnet, which is independent of the coupling λ and equivalent to $p \rightarrow \infty$.

While in both the site- and bond-centered cases (Figs. 6(a) and (b), respectively) the perpendicular velocity depends on the coupling ratio, in the bond-centered case v_\perp rapidly saturates to a value close to v_\parallel for large λ . As a consequence, the value of the coupling ratio $\lambda = J_b/J_a$ cannot be determined solely by the ratio of the acoustic velocities but requires additional information, such as v_{AF} .

The curves of v_\perp and v_\parallel cross at $\lambda = 1$ for the bond-centered case, apparently independent of p for the widths



(a) Acoustic spin wave velocities for VS3



(b) Acoustic spin wave velocities for VB3

FIG. 6: Spin wave velocities for (a) VS3 and (b) VB3 as a function of the coupling ratio λ . The solid curves in panel (a) are analytic results for VS3 calculated in Section IV B. Symbols in both (a) and (b) are numerical results. The velocities parallel and perpendicular to the stripe direction are equal to each other for $\lambda = 2/7$ and $\lambda = 1$ in the site- and bond-centered cases respectively. Qualitatively similar behavior is found for other stripe spacings.

we have studied. The crossing is at most weakly dependent on p in the site-centered case, occurring at $\lambda = 2/7$ for DS3, and at $\lambda = 0.3$ for DS4. For all spacings studied, we find that in the bond-centered case, v_\parallel is independent of the coupling λ and that v_\perp rapidly saturates with large λ . As p gets larger, both of these velocities approach v_{AF} . For the VB3 configuration, $v_\parallel = 0.9v_{AF}$, independent of λ . Notice that the independence of v_\parallel upon λ and the rapid saturation of v_\perp as λ becomes larger than 1 means that bond-centered configurations can produce rather isotropic spin wave cones.^{3,4}

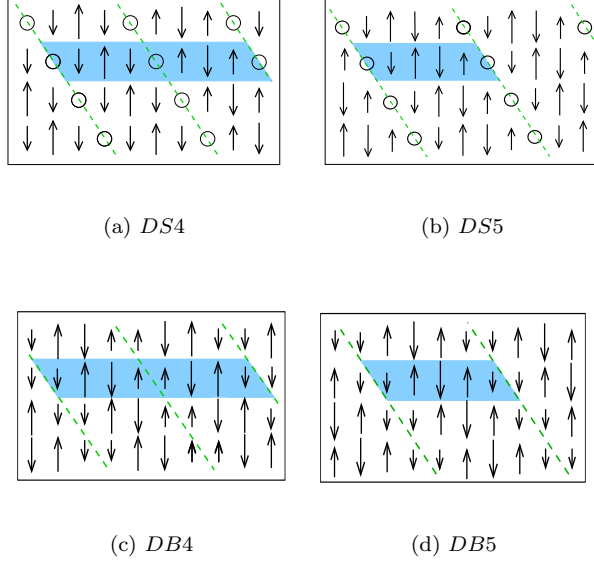


FIG. 7: (Color online) Diagonal site- and bond-centered configurations, showing even and odd spacing. Dotted lines denote domain walls. Solid parallelograms denote unit cells.

V. RESULTS FOR DIAGONAL STRIPES

Fig. 7 depicts representative diagonal configurations, for site- and bond-centered domain walls and with even and odd spacing. As mentioned in Sec II B, for a given microscopic model, diagonal stripes are more strongly coupled across the domain wall than vertical stripes. In addition, there are more parameters to consider for site-centered diagonal stripes: we must include J_c as well as J_b (see Fig. 1), since both couplings appear to the same order if derived from, *e.g.*, a Hubbard-like model.

A. Elastic Peak at $(0,0)$

Like their vertical counterparts, *bond-centered* diagonal stripes can produce new peaks in the elastic response. With diagonal stripes the new weight is physically transparent. For all bond-centered domain walls, nearest-neighbor spins are ferromagnetically coupled across the wall, and in the diagonal case, nearest neighbor pairs *along* a single domain wall all have their moments pointing in the same direction, leading to a domain wall magnetization. As Fig (7) illustrates, for diagonal stripes with even p , adjacent domain walls have alternating signs of the magnetization. But diagonal stripes with odd spacing have the same magnetization direction on each domain wall. This generically leads to net ferromagnetism and a peak at $(0,0)$, unless parameters are fine-tuned. In a three dimensional antiferromagnet, (as may happen,¹⁷ *e.g.*, with weakly coupled planes) domain walls are two dimensional (planar), and this peak appears ei-

ther at $(0,0,\pi)$ if the diagonal in-plane stripes lie directly on top of each other from plane to plane (meaning there is also no net magnetization on a domain wall), or at $(0,0,0)$ if the stripes are diagonal within a plane and in their correlation from plane to plane.

B. Analytic results for small p

As for the case of vertical stripes discussed in Sec. IV B, for small p , it is possible to obtain analytic forms for the acoustic dispersion relations for diagonal stripes in both the site- and bond-centered cases.

For the case DS3, the analytic dispersion is

$$\begin{aligned} \left(\frac{\omega_{DS3}}{J_a S}\right)^2 / 2 &= f(k_x - k_y) + \lambda^2 f(2(k_x - k_y)) \\ &+ 2\lambda\lambda_c f(k_x - k_y) \\ &+ (\lambda + \lambda_c)[f(2k_x + k_y) + f(k_x + 2k_y)] \\ &+ \lambda[f(3k_x) + f(3k_y)], \end{aligned} \quad (20)$$

$$(21)$$

where $\lambda_c = |\frac{J_c}{J_a}|$, and where the function f is defined as

$$f(x) = 1 - \cos(x), \quad (22)$$

as in Sec. IV B.

The dispersion perpendicular to the stripes, along the $\mathbf{k} = (k_x, k_x)$ direction, is then

$$\frac{\omega(k_x, k_x)}{J_a S} = \sqrt{8(2\lambda + \lambda_c)} \left| \sin\left(\frac{3k_x}{2}\right) \right|, \quad (23)$$

which yields for the velocity in that direction

$$v_{\perp} = \frac{3\sqrt{2\lambda + \lambda_c}}{2\sqrt{2}} v_{AF}, \quad (24)$$

which approaches $v_{\perp} \rightarrow \frac{3}{2}\sqrt{2\lambda} v_{AF}$ for large λ , and $v_{\perp} \rightarrow \frac{3}{2}\sqrt{\lambda_c} v_{AF}$ for large λ_c .

In the parallel direction $(k_x, -k_x)$, the dispersion becomes

$$\begin{aligned} \frac{1}{8} \left(\frac{\omega(k_x, -k_x)}{J_a S} \right)^2 &= (1 + \lambda + \lambda_c + \cos k_x + \lambda \cos(2k_x)) \\ &\times (1 + 2\lambda + 2\lambda \cos k_x) \sin^2 \frac{k_x}{2}, \end{aligned} \quad (25)$$

$$(26)$$

which gives

$$v_{\parallel} = \frac{\sqrt{(1 + 4\lambda)(2 + 2\lambda + \lambda_c)}}{2\sqrt{2}} v_{AF}. \quad (27)$$

This approaches $v_{\parallel} \rightarrow \lambda v_{AF}$ for large λ , and $v_{\parallel} \rightarrow \sqrt{\lambda_c/8} v_{AF}$ for large λ_c .

For the case DB2, the analytic dispersion is

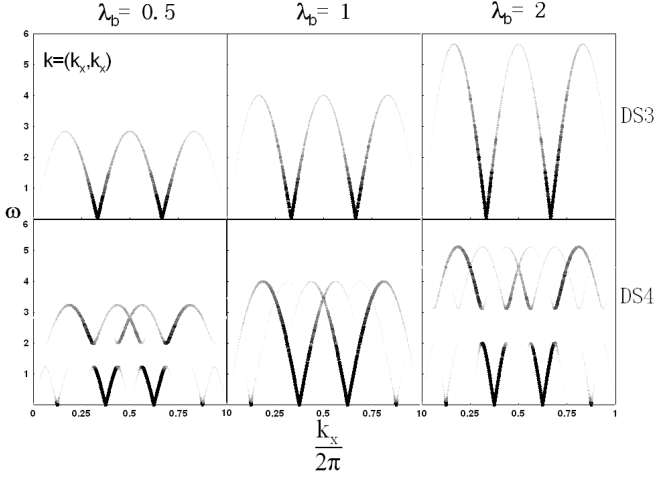


FIG. 8: Dispersion and intensities for DS3 and DS4 along (k_x, k_x) direction with J_b only. The frequency ω is in units of $J_a S$. For all plots, $J_c = 0$.

$$\left(\frac{\omega_{DB2}}{J_a S}\right)^2 / 2 = 4\lambda(1 + \lambda) + A - \lambda\sqrt{16(1 + \lambda)^2 + B} \quad (28)$$

where

$$\begin{aligned} A &= (1 - \lambda^2)f(k_x - k_y) \\ B &= -8(1 + \lambda)^2 f(k_x - k_y) \\ &\quad + (2 - f(k_x - k_y)) [2f(k_x - k_y) \\ &\quad - 2f(2k_x - 2k_y) - f(3k_x + k_y) - f(k_x + 3k_y)] . \end{aligned} \quad (29)$$

Perpendicular to the stripes, along $\mathbf{k} = (k_x, k_x)$, the velocity is

$$v_{\perp} = \sqrt{\frac{\lambda}{\lambda + 1}} v_{AF} , \quad (30)$$

saturating to $v_{\perp} \rightarrow v_{AF}$ as $\lambda \gg 1$. In the direction $\mathbf{k} = (k_x, -k_x)$, parallel to the stripes, the velocity is

$$v_{\parallel} = \frac{1}{2} \sqrt{\lambda + 1} v_{AF} . \quad (31)$$

C. Numerical Results

In Fig. 8, we plot the dispersion and intensities for DS3 and DS4 along (k_x, k_x) for various values of the coupling ratio $\lambda = |J_b/J_a|$, setting $J_c = 0$. (See Fig. 1 for the definitions of J_b and J_c .) Similar results using a J_c only model (*i.e.* with $J_b = 0$) are reported in Ref.²⁴. Our results show similar band structures but with critical coupling $\lambda = 1$, which is only half of the J_c only model.

However, the effects of J_b and J_c depend upon the direction in k space. In Fig. 9 we show the effects of varying the couplings J_b and J_c for two cuts in momentum space for DS3. For a cut perpendicular to the stripe

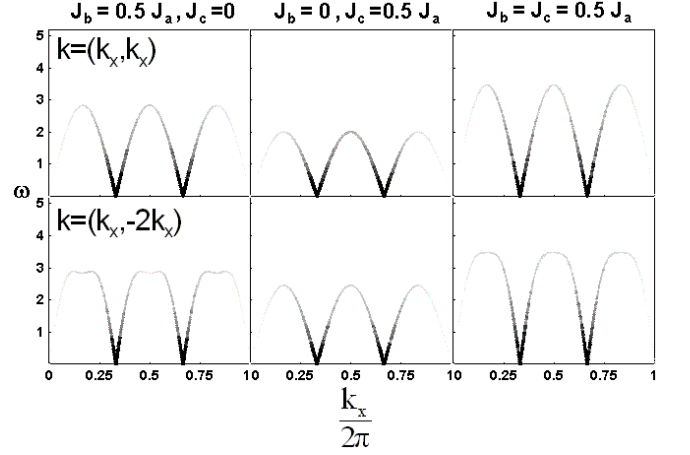


FIG. 9: Dispersion and intensities for DS3 along (k_x, k_x) and $(k_x, -2k_x)$ directions, comparing the effects of J_b and J_c . The frequency ω is in units of $J_a S$.

direction, J_b and J_c have more or less the same effect, although since J_b couples more spins than J_c , it has a more dramatic effect. Increasing either coupling broadens the bandwidth in a roughly linear manner with negligible effect on the shape. However, for the cut $(k_x, -2k_x)$, we see that the presence of J_b produces inflection points when $J_c = 0$, and can produce flat-topped dispersions if J_c is included as well.

We show in Fig. 10 the calculated dispersion relations and intensities for the bond-centered diagonal case, for spacings $p = 2, 3$, and 4. As in the vertical case, the number of bands is equal to p . A striking difference in the spectra of odd spacings is seen, as the net ferromagnetism in the system changes the low-energy character of the spin waves from a linear (antiferromagnetic-like) to a quadratic (ferromagnetic-like) dispersion. Rather than the band repulsion observed in the vertical case (except at finely tuned values of the coupling), crossing of optical bands is generic in the bond-centered diagonal case. Note the ability of optical bands to cross, indicating a difference in symmetry for the crossing bands. Also evident in the dispersion of DB4 is the downturn of the acoustic band at $2p$ magnetic reciprocal lattice vectors, twice as many as in the odd case. (See Sec. II B.) This is expected because of the doubling of the unit cell necessary to accommodate even spacing. Note, however, that spectral weight is forbidden at these extra reciprocal lattice vectors, including the (π, π) point.

In Fig. 11, we plot the spin wave velocities for DS3. When J_b and J_c are both finite, there is a wide range of couplings λ for which the spin wave velocities parallel and perpendicular to the stripes are nearly equal, while this approximate isotropy is confined to a narrow range of λ if either J_b or J_c is zero. Fig. 12, which presents v_{\perp} and v_{\parallel} for the case DB4, shows the characteristic saturation of v_{\perp} with large λ for bond-centered stripes.

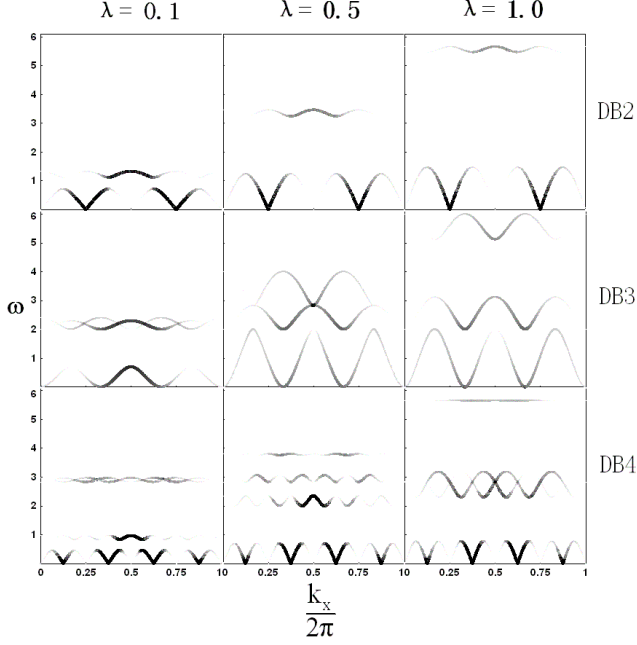


FIG. 10: Dispersion and intensities for diagonal bond-centered domain walls along (k_x, k_x) direction, at $\lambda = 0.1, 0.5, 1.0$, for $p = 2, 3$, and 4 . The frequency ω is in units of $J_a S$.

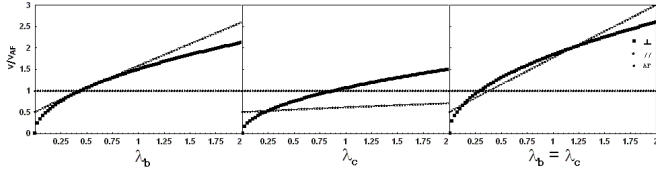


FIG. 11: Velocities parallel ($v_{||}$) and perpendicular (v_{\perp}) to the stripe direction, as compared to v_{AF} , for DS3. In the first panel, $J_c = 0$, and the velocities are plotted as a function of $\lambda_b = J_b/J_a$. In the second panel, $J_b = 0$, and the velocities are plotted as a function of $\lambda_c = J_c/J_a$. In the third panel, $J_b = J_c$, and the velocities are plotted as a function of $\lambda_b = \lambda_c$.

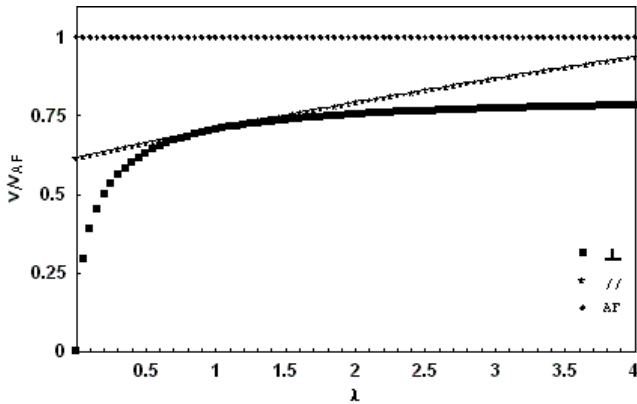


FIG. 12: Velocities parallel ($v_{||}$) and perpendicular (v_{\perp}) to the stripe direction, as compared to v_{AF} , for DB4.

VI. EXPERIMENTAL IMPLICATIONS

We have shown that for a certain class of nontrivial spin orderings on a lattice, the spin wave response is sensitive to the microscopic placement of the antiphase domain walls. Furthermore, even elastic neutron scattering can in principle distinguish site- from bond-centered for odd stripe spacings, whether vertical or diagonal.

While both site- and bond-centered odd width vertical stripe configurations will produce elastic weight at $(\pi \pm \frac{\pi}{p}, \pi)$, only configurations that are phase-shifted from the site-centered configuration (*e.g.* a bond-centered configuration) are capable of producing weight at $(0, \pi)$, and the observation of this peak along with peaks at $(\pi \pm \frac{\pi}{p}, \pi)$ would rule out a site-centered vertical configuration. A similar ferromagnetic peak—*i.e.*, at $(0, 0)$ —would rule out site-centered diagonal stripes.¹⁷

Figs. 6 and 12 illustrate another important implication for experiments: The transverse spin wave velocity v_{\perp} in the acoustic band *saturates* for large λ in the bond-centered case for both vertical and diagonal stripes. In fact, all but the top band in the bond-centered case saturate and become *independent* of J_b for large J_b . As noted above, this unfortunately means that an estimate of $\lambda = J_b/J_a$ cannot necessarily be discerned directly from the ratio $v_{\perp}/v_{||}$ but requires either independent knowledge of whether the stripes are site- or bond-centered, or an appropriate estimate of the bare coupling (from, *e.g.* v_{AF}).

A prominent piece of phenomenology in the cuprates is the “resonance peak” observed in neutron scattering,^{27,28,29} which is the presence of extra scattering weight appearing at (π, π) at finite frequency, typically of order $40 meV$. One proposal is that this may be due to spin waves crossing.^{30,31} We note that for vertical stripes, spin waves generically repel and appear to cross only at finely tuned values of the coupling. For site-centered configurations, this corresponds to $\lambda = 1$ and $\lambda \approx 2.5$, while for bond-centered configurations, the critical coupling is near $\lambda \approx 0.56$. However, a finite energy resolution measurement would not be able to distinguish actual crossings from near crossings. In the bond-centered case with large λ , the first optical mode has more weight at (π, π) than the acoustic band, which would tend to leave the weight near the elastic incommensurate peaks $(\pi \pm \frac{\pi}{p}, \pi)$ rather disconnected from what might be called a “resonance peak” in this configuration. We also note that our calculations show that band crossings are more generic in the presence of diagonal stripes than vertical stripes.

The nickelate compound $\text{La}_{1.69}\text{Sr}_{0.31}\text{NiO}_4$ shows evidence from neutron scattering of diagonal stripes with spacing $p = 3$.^{3,4} As Sr is substituted for La, holes are doped into the NiO_2 planes. Neutron scattering has been used to map out the acoustic spin wave dispersion for this material. The data reveal rather isotropic spin wave cones, *i.e.* that v_{\perp} and $v_{||}$ are rather similar, with

$v_{\perp} \approx (1.03 \pm 0.06)v_{AF}$ and $v_{\parallel} \approx (0.86 \pm 0.06)v_{AF}$,³ where v_{AF} is the acoustic spin wave velocity of the undoped antiferromagnet. For the DS3 state, if we include *only* J_b or *only* J_c , we find no coupling strength λ for which these two relations can be simultaneously satisfied. The presence of the two couplings together, as shown in Fig. 11 with $J_b = J_c$, can account for the proper relationship among the velocities, but only for a small range of rather small coupling ratio. As a general trend, we find approximate isotropy of the spin wave cones to be more robust for bond-centered stripes (in both vertical and diagonal cases), and so one might suspect bond-centered stripes could be responsible for the near isotropy of the spin waves in this material. However, as we have shown, the DB3 configuration yields a ferromagnetic spin wave dispersion, which is certainly not supported by the data.

In the related compound $\text{La}_2\text{NiO}_{4.133}$ ¹⁷, signatures of spin stripes have been detected in neutron scattering. “Incommensurate peaks” are observed to persist up to a temperature T_m , above which magnetic peaks indicative of stripe structure can be regained by application of a 6T magnetic field. The field-induced stripe spacing (both above and slightly below T_m) is smaller than the zero-field stripe spacing observed below T_m . As noted by the authors,¹⁷ the ferrimagnetic response is naturally explained by bond-centered stripes. In the high temperature field-induced stripe phase, the diagonal stripes have spacing $p = 3$. Our results in Fig. 10 suggest that this field-induced transition should be accompanied by a dramatic change in the low-energy spin wave dispersion, from linear to quadratic.

We have also shown that (as in the site-centered case²⁴) the number of bands in a bond-centered configuration is set by the number of spins in the unit cell, rather than by the spacing p . Generally, for both vertical and diagonal stripes, site-centered stripes have $(p - 1)$ spin wave bands, and bond-centered stripes have p bands. The exception is the case of diagonal site-centered stripes with odd spacing p , which has $\frac{1}{2}(p - 1)$ bands. An experimental consequence of this is that for a given value of p , bond-centered stripes have p spin wave bands, whereas site-centered stripes have at most $p - 1$ bands. Although not yet observed experimentally, this means that the upper bands can also be used to distinguish site- from bond-centered stripes. Finding p bands along with incommensurate peaks indicative of spacing p would rule out site-centered stripes. For diagonal odd width stripes, the threshold is even lower. For, *e.g.*, DS3, only one spin wave band is expected, whereas for DB3, we expect to find three bands. The observance of a second band (or equivalently a spin wave crossing) for diagonal $p = 3$ stripes would rule out a site-centered configuration. Of course, negative evidence is dicier, and the observance of the smaller number of bands cannot distinguish the two, as it cannot rule out the possibility that the top band is too faint to be observed.

VII. CONCLUSIONS

In conclusion, we have studied regular arrays of antiphase domain walls in two-dimensional Heisenberg antiferromagnets and find that their location relative to the lattice—*i.e.*, whether they are site-centered or bond-centered—produces distinct effects which may be measurable in a diffraction probe such as neutron scattering. In particular, arrays of odd-width, bond-centered antiphase domain walls generically produce more elastic peaks than site-centered stripes. In addition, bond-centered stripes generically produce more bands than site-centered stripes. We further find that low-energy spin wave velocities are not always directly related to the exchange couplings in the model, and in particular for bond-centered configurations, rather isotropic spin wave cones are predicted for a wide range of parameters.

Acknowledgements

It is a pleasure to thank I. Affleck, A. Castro Neto, S. Kivelson, B. Lake, Y. S. Lee, S. Rosenkranz, A. Sandvik, and J. Tranquada for helpful discussions. This work was supported by the U.S. Government and by Boston University.

APPENDIX A: SPIN-WAVE METHODS

We rewrite the Hamiltonian Eqn. (1) using the ladder operators:

$$H = \frac{1}{2} \sum_{\langle \mathbf{r}, \mathbf{r}' \rangle} J_{\mathbf{r}, \mathbf{r}'} [S_{\mathbf{r}}^z S_{\mathbf{r}'}^z + \frac{1}{2} (S_{\mathbf{r}}^+ S_{\mathbf{r}'}^- + S_{\mathbf{r}}^- S_{\mathbf{r}'}^+)]. \quad (\text{A1})$$

We now replace the spin operators by Holstein-Primakoff (HP) bosons³²

$$\begin{aligned} S_i^+ &= \sqrt{2S} a_i \\ S_i^- &= \sqrt{2S} a_i^+ \\ S_i^z &= S - a_i^+ a_i \end{aligned} \quad (\text{A2})$$

for odd sites i occupied by a spin up, and

$$\begin{aligned} S_i^+ &= \sqrt{2S} a_i^+ \\ S_i^- &= \sqrt{2S} a_i \\ S_i^z &= -S + a_i^+ a_i \end{aligned} \quad (\text{A3})$$

for even sites i occupied by a spin down. Here, i labels each spin within a unit cell, *i.e.* $i = 1, 2, \dots, N$, where N is the number of spins in the unit cell. We use odd i to represent $S_z = \uparrow$ spins and even i for $S_z = \downarrow$ spins. We Fourier transform the bosonic operators via

$$\begin{aligned} a_i(\mathbf{k}) &= \frac{1}{\sqrt{n}} \sum_{\mathbf{r} \in \text{odd } i} a_{\mathbf{r}} e^{i\mathbf{k} \cdot \mathbf{r}}, \\ a_j(\mathbf{k}) &= \frac{1}{\sqrt{n}} \sum_{\mathbf{r} \in \text{even } i} a_{\mathbf{r}} e^{-i\mathbf{k} \cdot \mathbf{r}}. \end{aligned} \quad (\text{A4})$$

Finally, we get the Hamiltonian in momentum space

$$H = \sum_{ij} A_{i,j} a_i^+(\mathbf{k}) a_j(\mathbf{k}) + \frac{1}{2} \sum_{ij} [B_{ij} a_i^+(\mathbf{k}) a_j^+(\mathbf{k}) + B_{ij}^* a_j(\mathbf{k}) a_i(\mathbf{k})], \quad (\text{A5})$$

where $A = A^+$ and $B^T = B$.

The quadratic Hamiltonian (A5) can be diagonalized via a canonical symplectic transformation³³ T , $b = Ta$, using the bosonic metric

$$\eta = \begin{pmatrix} I & 0 \\ 0 & -I \end{pmatrix}, \quad (\text{A6})$$

where I is the $N \times N$ identity matrix. This leads to

$$H(\mathbf{k}) = \sum_{\alpha} [b_{\alpha}^+(\mathbf{k}) \omega_{\alpha}(\mathbf{k}) b_{\alpha}(\mathbf{k}) + \frac{1}{2} \omega_{\alpha}(\mathbf{k})]. \quad (\text{A7})$$

We now consider the structure factor. Only S^x and S^y contribute to the inelastic part of the structure factor. In terms of HP bosons,

$$\begin{aligned} S_{\mathbf{k}}^x &= \frac{1}{2} (S_{\mathbf{k}}^+ + S_{\mathbf{k}}^-) \\ &= \sqrt{\frac{S}{2}} \left(\sum_{i \in \text{odd}} [a_i^+(-\mathbf{k}) + a_i(\mathbf{k})] \right. \\ &\quad \left. + \sum_{i \in \text{even}} [a_i^+(\mathbf{k}) + a_i(-\mathbf{k})] \right) \end{aligned} \quad (\text{A8})$$

We then substitute Eqn. (A8) into the structure factor and keep only the creation operators $\{b_1^+(\mathbf{k}), b_2^+(\mathbf{k}), \dots\}$, which connect the vacuum to singly excited states. This gives

$$\begin{aligned} S^{in}(\mathbf{k}, \omega_{\alpha}) &= 2 \sum_f |\langle f | S_{\mathbf{k}}^x | 0 \rangle|^2 \delta(\omega - \omega_f) \\ &= |S| < 1 | (\sum_i \alpha_i b_i^+) | 0 \rangle|^2 \\ &= |S| \sum_i |\alpha_i|^2, \end{aligned} \quad (\text{A9})$$

where α_i is the i th component of the (orthonormalized) eigenvector $|\alpha\rangle$ of the Hamiltonian using the bosonic metric, corresponding to eigenvalue ω_{α} .

APPENDIX B: DIMERIZED SPIN MODEL

We consider an isolated system of two spins with ferromagnetic coupling J_b . In the ground state, the two spins are aligned. When the spins tilt a bit, each produces an effective field acting on the other. Using the classical spin wave method, we have

$$\begin{aligned} \frac{d\mathbf{S}_1}{dt} &= -\frac{J_b}{\hbar} \mathbf{S}_1 \times \mathbf{S}_2 \\ \frac{d\mathbf{S}_2}{dt} &= -\frac{J_b}{\hbar} \mathbf{S}_2 \times \mathbf{S}_1 \end{aligned} \quad (\text{B1})$$

Ignoring the change in S_z , the x, y components of the two spins satisfy

$$\begin{aligned} \frac{dS_1^x}{dt} &= -\frac{dS_2^x}{dt} = -\frac{J_b S}{\hbar} (S_1^y - S_2^y) \\ \frac{dS_1^y}{dt} &= -\frac{dS_2^y}{dt} = \frac{J_b S}{\hbar} (S_1^x - S_2^x). \end{aligned} \quad (\text{B2})$$

Integrating yields $S_1^{x,y} = -S_2^{x,y} + c$, where c is a constant of integration. Since we allow only S_z to have a constant component, $c = 0$. Taking the second derivative of S_1^x , we find

$$\begin{aligned} \frac{d^2 S_1^x}{dt^2} &= -\frac{J_b S}{\hbar} \left(\frac{dS_1^y}{dt} - \frac{dS_2^y}{dt} \right) \\ &= -\frac{J_b S}{\hbar^2} [J_b S (S_1^x - S_2^x) + J_b S (S_1^x - S_2^x)] \\ &= -2 \frac{J_b^2 S^2}{\hbar^2} [S_1^x - S_2^x] \\ &= -4 \frac{J_b^2 S^2}{\hbar^2} S_1^x, \end{aligned} \quad (\text{B3})$$

which is a harmonic oscillator equation. If we set $S_1^x(x, t) = u(x) e^{i\omega t}$, we see that the oscillation frequency is

$$\omega = 2 \frac{|J_b|}{\hbar} S, \quad (\text{B4})$$

which recovers the large J_b limit of Eqn. 15.

¹ J. M. Tranquada, AIP Conf. Proc. **483**, 336 (1999).

² P. Dai, H. A. Mook, and F. Dogan, Phys. Rev. Lett. **80**, 1738 (1998).

³ P. Bourges, Y. Sidis, M. Braden, K. Nakajima, and J. M. Tranquada, Phys. Rev. Lett. **90**, 147202 (2003).

⁴ A. T. Boothroyd, D. Prabhakaran, P. G. Freeman, S. J. S. Lister, M. Enderle, A. Hiess, and J. Kulda, Phys. Rev. B

67, 100407 (2003).

⁵ A. T. Boothroyd, P. G. Freeman, D. Prabhakaran, A. Hiess, M. Enderle, J. Kulda, and F. Altorfer, Phys. Rev. Lett. **91**, 257201 (2003).

⁶ V. J. Emery, S. A. Kivelson, and O. Zachar, Phys. Rev. B **56**, 6120 (1997).

⁷ J. Zaanen, Nature **404**, 714 (2000).

- ⁸ J. Ye and S. Sachdev, Phys. Rev. B **44**, 10173 (1991).
- ⁹ D. J. Scalapino and S. R. White, Found. Phys. **31**, 27 (2001).
- ¹⁰ R. S. Markiewicz and M. T. Vaughn, J. Phys. Chem. Sol. **59**, 1737 (1998).
- ¹¹ A. H. Castro Neto, Phys. Rev. B **64**, 104509 (2001).
- ¹² E. Kaneshita, M. Ichioka, and K. Machida, J. Phys. Soc. Jpn. **70**, 866 (2001).
- ¹³ Here we follow the convention of the literature, and express the wavevector in units where the lattice spacing $a = 1$.
- ¹⁴ H. A. Mook, P. C. Dai, F. Dogan, and R. D. Hunt, Nature **404**, 729 (2000).
- ¹⁵ S. Wakimoto, J. M. Tranquada, T. Ono, K. M. Kojima, S. Uchida, S. H. Lee, P. M. Gehring, and R. J. Birgeneau, Phys. Rev. B **64**, 174505 (2001).
- ¹⁶ We follow the convention of the literature, and refer to satellite peaks around (π, π) as incommensurate peaks, even though they may be commensurate with the underlying lattice.
- ¹⁷ J. M. Tranquada, P. Wochner, A. R. Moodenbaugh, and D. J. Buttrey, Phys. Rev. B **55**, R6113 (1997).
- ¹⁸ S. A. Kivelson, E. Fradkin, V. Oganesyan, I. P. Bindloss, J. M. Tranquada, A. Kapitulnik, and C. Howald, Rev. Mod. Phys. (2003), cond-mat/0210683.
- ¹⁹ O. Zachar, S. A. Kivelson, and V. J. Emery, Phys. Rev. B **57**, 1422 (1998).
- ²⁰ J. Zaanen, M. L. Horbach, and W. vanSaarloos, Phys. Rev. B **53**, 8671 (1996).
- ²¹ S. R. White and D. J. Scalapino, Phys. Rev. Lett. **81**, 3227 (1998).
- ²² N. Ichikawa, S. Uchida, J. M. Tranquada, T. Niemoller, P. M. Gehring, S. H. Lee, and J. R. Schneider, Phys. Rev. Lett. **85**, 1738 (2000).
- ²³ In the physical system, holes residing on the domain wall do carry spin, and they may under certain conditions lead to a net spin on the domain walls as well. However, this is a secondary order parameter which generically can order only after the spin texture we describe, and we leave its description to future work.
- ²⁴ F. Kruger and S. Scheidl, Phys. Rev. B **67**, 134512 (2003).
- ²⁵ D. Goodstein, *States of Matter* (Prentice-Hall, Englewood Cliffs, N.J., 1975).
- ²⁶ G. L. Squires, *Introduction to the Theory of Thermal Neutron Scattering* (Dover, Mineola, NY, 1997).
- ²⁷ H. F. Fong, B. Keimer, P. W. Anderson, D. Reznik, F. Dogan, and I. A. Aksay, Phys. Rev. Lett. **75**, 316 (1995).
- ²⁸ P. Dai, H. A. Mook, R. D. Hunt, and F. Dogan, Phys. Rev. B **63**, 054525 (2001).
- ²⁹ J. Rossat-Mignod, L. P. Regnault, C. Vettier, P. Bourges, P. Burlet, J. Bossy, J. Y. Henry, and G. Lapertot, Physica C **185-189**, 86 (1991).
- ³⁰ A. V. Balatsky and P. Bourges, Phys. Rev. Lett. **82**, 5337 (1999).
- ³¹ C. D. Batista, G. Ortiz, and A. V. Balatsky, Phys. Rev. B **64**, 172508 (2001).
- ³² A. Auerbach, *Interacting Electrons and Quantum Magnetism* (Springer-Verlag, New York, 1994).
- ³³ J.-P. Blaizot and G. Ripka, *Quantum Theory of Finite Systems* (MIT Press, Cambridge, Mass., 1986).